Science of the Total Environment 765 (2021) 144263

Contents lists available at ScienceDirect

Science of the Total Environment

journal homepage: www.elsevier.com/locate/scitotenv

Constructing a spatiotemporally coherent long-term $PM_{2.5}$ concentration dataset over China during 1980–2019 using a machine learning approach

Huimin Li [a], Yang Yang [a,*], Hailong Wang [b], Baojie Li [a], Pinya Wang [a], Jiandong Li [a], Hong Liao [a]

[a] Jiangsu Key Laboratory of Atmospheric Environment Monitoring and Pollution Control, Jiangsu Collaborative Innovation Center of Atmospheric Environment and Equipment Technology, School of Environmental Science and Engineering, Nanjing University of Information Science and Technology, Nanjing, Jiangsu, China
[b] Atmospheric Sciences and Global Change Division, Pacific Northwest National Laboratory, Richland, WA, USA

HIGHLIGHTS

- Long-term $PM_{2.5}$ is essential due to the coverage deficiency of surface observations.
- A machine learning model with visibility and many auxiliary data inputs is applied.
- A 1-degree gridded daily $PM_{2.5}$ dataset over China for 1980–2019 is constructed.
- The model performs well with a high coefficient of determination and low bias.
- It will be a promising tool for assessing related impacts on environment and climate.

GRAPHICAL ABSTRACT

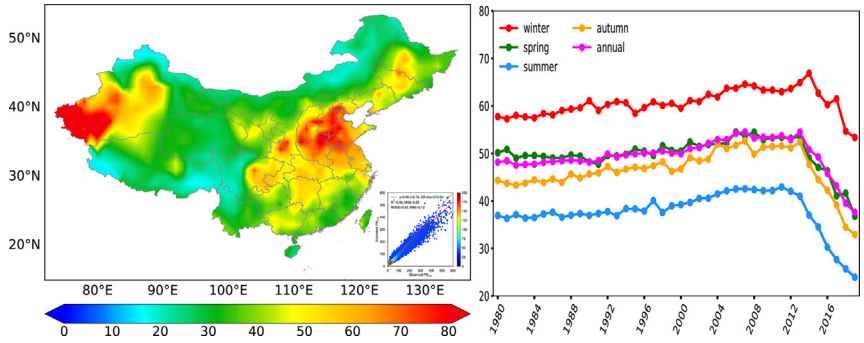

ARTICLE INFO

Article history:
Received 2 October 2020
Received in revised form 27 November 2020
Accepted 27 November 2020
Available online 24 December 2020

Editor: Pingqing Fu

Keywords:
Fine particulate matter
Space-time random forest model
Atmospheric visibility
Spatial and temporal variation
Clean air actions

ABSTRACT

The lack of long-term observations and satellite retrievals of health-damaging fine particulate matter in China has demanded the estimates of historical $PM_{2.5}$ (particulate matter less than 2.5 μm in diameter) concentrations. This study constructs a gridded near-surface $PM_{2.5}$ concentration dataset across China covering 1980–2019 using the space-time random forest model with atmospheric visibility observations and other auxiliary data. The modeled daily $PM_{2.5}$ concentrations are in excellent agreement with ground measurements, with a coefficient of determination of 0.95 and mean relative error of 12%. Besides the atmospheric visibility which explains 30% of total importance of variables in the model, emissions and meteorological conditions are also key factors affecting $PM_{2.5}$ predictions. From 1980 to 2014, the model-predicted $PM_{2.5}$ concentrations increased constantly with the maximum growth rate of 5–10 $\mu g/m^3$/decade over eastern China. Due to the clean air actions, $PM_{2.5}$ concentrations have decreased effectively at a rate over 50 $\mu g/m^3$/decade in the North China Plain and 20–50 $\mu g/m^3$/decade over many regions of China during 2014–2019. The newly generated dataset of 1-degree gridded $PM_{2.5}$ concentrations for the past 40 years across China provides a useful means for investigating interannual and decadal environmental and climate impacts related to aerosols.

1. Introduction

Particulate matter is one of the major health-damaging components in the atmosphere, especially those with the aerodynamic diameters smaller than 2.5 μm ($PM_{2.5}$). Long-term exposure to $PM_{2.5}$ can increase

* Corresponding author.
E-mail address: yang.yang@nuist.edu.cn (Y. Yang).

https://doi.org/10.1016/j.scitotenv.2020.144263
0048-9697/

risks of many adverse health issues, including respiratory and cardiovascular diseases, lung cancer and premature death (Crouse et al., 2012; Pope et al., 2002; Xing et al., 2016; Zhang et al., 2017). The presence of high concentrations of $PM_{2.5}$ also reduces atmospheric visibility, influences the public transportation, and thus adversely affects social and economic activities (Zhang et al., 2014). These aerosol particles also influence climate via aerosol-radiation and aerosol-cloud interactions (Boucher et al., 2013; Yang et al., 2020). Through long-range transport, the local environmental and climatic impacts of aerosols near major source regions can be extended globally (Ren et al., 2020; Wang et al., 2014).

Aerosol concentrations in China are experiencing great changes in recent decades. The rapid industrial development and urbanization were primarily responsible for the increasing tendency of $PM_{2.5}$ concentrations before 2010 (Yang et al., 2016; Cohen et al., 2017). From 2013 to 2017, the PM pollution was alleviated, with the national averaged concentration reduced by one third, primarily owing to the implementation of clean air actions in China (Huang et al., 2018). Following the growing public health concern, many air quality monitoring stations have been established to measure real-time $PM_{2.5}$ concentrations since 2013. However, the measurements are limited to a short temporal coverage and have uneven spatial distributions (Wang et al., 2019; Zhao et al., 2020), so they are insufficient to describe the long-term characteristics of $PM_{2.5}$ in China. Because the spatiotemporal variation of $PM_{2.5}$ and its relationship with changes in emissions, weather and climate can be used to improve the current understanding of pollution formation and provide the scientific basis of air quality improvement to policy makers, it is essential to produce a long-term dataset of gridded surface $PM_{2.5}$ concentrations based on real observed data in China.

To overcome the spatiotemporal coverage deficiency of surface $PM_{2.5}$ observations, satellite remote sensing data have been widely used to estimate surface $PM_{2.5}$ concentrations recently (Fang et al., 2016; Wei et al., 2019). In general, aerosol optical depth (AOD) derived from satellite has a positive correlation with near-surface $PM_{2.5}$ concentrations. Based on this, a variety of statistical models, including multiple linear regression (Chelani, 2019), geographically weighted regression (Ma et al., 2014; Guo et al., 2017), linear mixed-effect model (Zheng et al., 2016), and two-stage model (Ma et al., 2016; Yao et al., 2019), have been applied to assess $PM_{2.5}$. In addition, machine learning has become a modern tool for a regression task nowadays due to its computational efficiency and state-of-the-art performance (Stafoggia et al., 2019). Wei et al. (2019) produced $PM_{2.5}$ concentrations at 1-km resolution in China for 2016 based on satellite AOD using the space-time random forest (STRF) model, with a cross-validation (CV) coefficient of determination (R^2) of 0.85. Li et al. (2017) estimated $PM_{2.5}$ in 2015 over China using a geo-intelligent deep learning model together with satellite AOD data, in which the CV R^2 increases from 0.42 to 0.88 relative to the traditional neural network method. However, these estimated $PM_{2.5}$ data still have some limitations in certain aspects. First of all, the Moderate Resolution Imaging Spectroradiometer (MODIS) data were not available until 1999 and Suomi National Polar-orbiting Partnership (S-NPP) satellite was launched in 2011. Most of the studies mentioned above used AOD derived from these two satellites to predict $PM_{2.5}$, and consequently the $PM_{2.5}$ data are not available before 2000 (van Donkelaar et al., 2015; Xue et al., 2019). Additionally, AOD represents aerosol loading in the entire atmospheric column and its relationship with near-surface $PM_{2.5}$ concentrations is largely influenced by planetary boundary layer height, relative humidity, temperature, and other factors (Liu et al., 2009). Moreover, algorithm bias, signal uncertainty, and cloud contamination induce biases to the $PM_{2.5}$ estimation from AOD (Stafoggia et al., 2019; Xiao et al., 2017).

Atmospheric visibility measurements, which have been available for several decades in China, were demonstrated to be a promising alternative for estimating near-surface $PM_{2.5}$ concentrations (Shen et al., 2016). Li et al. (2020) derived $PM_{2.5}$ concentrations over North China in 2014 using the combination of visibility observations and GEOS-Chem model simulations and reported that the estimated $PM_{2.5}$ was highly correlated to surface observations in time and space, with a correlation coefficient of 0.96 and 0.79, respectively. Liu et al. (2017) estimated historical (1957–1964 and 1973–2014) $PM_{2.5}$ in China using visibility measurements and a statistical approach, and found that the model can accurately estimate $PM_{2.5}$ concentrations with the CV R^2 of 0.71. They also reported an increasing trend of 1.9 $\mu g/m^3$/decade averaged over China during 1957–2014. Due to the better abilities in dealing with non-linear and complex relationships between variables than traditional statistical approaches, machine learning methods can also be used in the visibility-$PM_{2.5}$ prediction. By using a machine learning model (the Extreme Gradient Boosting), Gui et al. (2020) constructed surface $PM_{2.5}$ concentrations in 2018 over China based on visibility and meteorological data, which offered the potential in reconstructing long-term $PM_{2.5}$ data in China with a machine learning method. Furthermore, in addition to visibility and meteorology, other factors such as emissions, topography, population and land use data, should be considered in the machine learning model to simulate $PM_{2.5}$ concentrations and spatiotemporal distributions.

In this study, we construct a gridded dataset of near-surface $PM_{2.5}$ concentrations across China covering 1980–2019 using the STRF model along with atmospheric visibility and other auxiliary data (e.g., meteorology, anthropogenic emissions, land use, topography, population density and spatiotemporal information), which have a longer time coverage and are more representative of the near-surface aerosols than the data based on satellite AOD. The performance of the STRF model in estimating $PM_{2.5}$ in China is evaluated and the long-term variations of $PM_{2.5}$ are characterized.

2. Materials and methods

2.1. Datasets

We utilize existing hourly observed surface $PM_{2.5}$ concentrations during recent years (2014–2019), long-term atmospheric visibility and auxiliary data (e.g., meteorological variables, anthropogenic emissions, land use, national population, topography, and geographic and time variables of observations). The sources and preprocessing of data are elaborated below.

2.1.1. Surface $PM_{2.5}$ observations

The hourly ground measurements of $PM_{2.5}$ concentrations were attained from the China National Environmental Monitoring Center (CNEMC, http://www.cnemc.cn) over 2014–2019. Overall, there are 1657 monitoring stations, mostly distributed in metropolis of eastern China (e.g., the North China Plain, Yangtze River Delta, Pearl River Delta and Sichuan Basin), while the coverage is very limited in western China and areas of low-population density (Fig. 1). The data have undergone quality control/quality assurance processes to exclude any invalid values caused by defective reporting and instruments (Barrero et al., 2015; Pant et al., 2016; Zhai et al., 2019). When calculating daily and monthly averages, at least 12 hourly values per day and 20 daily values per month are required, respectively.

2.1.2. Visibility monitoring measurements

The daily atmospheric visibility measurements over China were collected from the National Climatic Data Center (NCDC, https://www7.ncdc.noaa.gov/CDO/cdoselect.cmd) by averaging at least four synoptic monitoring data each day. Although there are 1328 visibility monitoring stations (Fig. 1), totally 383 sites have daily visibility data covering 1980–2019 provided by NCDC, which are evenly distributed across China and are used in this study. To rule out rainy and foggy days, the days with precipitation > 0 or relative humidity (RH) $> 90\%$ are removed from the daily visibility observations. The calculation of monthly visibility averages from daily data follows that of surface $PM_{2.5}$. Because the visibility observation transformed from manual observation to

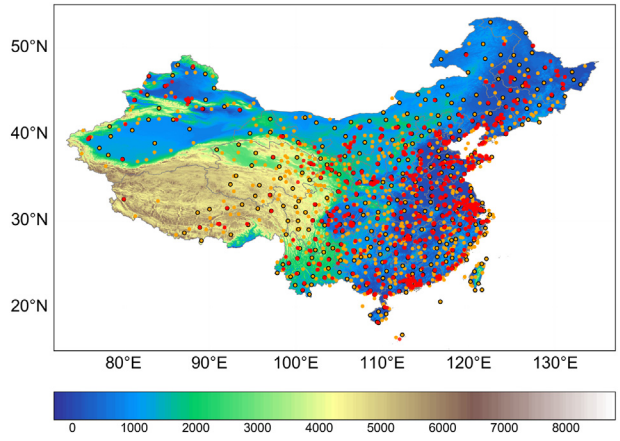

Fig. 1. Spatial distributions of $PM_{2.5}$ (red dots) and atmospheric visibility (orange dots) monitoring stations in China. The orange dots with black borders are 383 monitoring stations which have daily visibility covering 1980–2019 provided by NCDC. Topography (background colored shading, in meters) is from the SRTM DEM at a 90-m spatial resolution in 2015. (For interpretation of the references to colour in this figure legend, the reader is referred to the web version of this article.)

automatic monitoring across China around 2013–2014, following the guideline from China Meteorological Administration (CMA, 2014), in this study the atmospheric visibility data for 1980–2013 are multiplied by 0.75 for the calibration against those obtained after 2013.

2.1.3. Auxiliary data

Auxiliary data summarized in Table 1 include meteorological parameters, land use, topography, anthropogenic emissions, population, and spatiotemporal variables, which are the main factors affecting $PM_{2.5}$ (Yang et al., 2016; Wei et al., 2020; Zhao et al., 2020). RH is calculated according to the in-situ surface air temperature (TEMP) and dew point temperature measurements which are obtained from NCDC. The remaining meteorological variables, including the boundary layer height (BLH), surface pressure (SP), evaporation (ET), 10-m wind speed (WS) and wind direction (WD), are acquired from ERA5 reanalysis (https://www.ecmwf.int/en/forecasts/datasets/reanalysis-datasets/era5) at a horizontal resolution of 0.25° × 0.25° and temporal resolution of 6-h covering 1980–2019. Land-use data in year 2015, i.e., 300-m-resolution land cover and daily normalized difference vegetation index (NDVI) at a 0.05° × 0.05° resolution are obtained from the European Space Agency Climate Change Initiative (ESA CCI, http://maps.elie.ucl.ac.be/CCI/viewer/download.php) and the Advanced Very High Resolution Radiometer (AVHRR, https://www.ncei.noaa.gov/data/avhrr-land-normalized-difference-vegetation-index/access/), respectively. Topography data were collected from the Shuttle Radar Topography Mission (SRTM) Digital Elevation Model (DEM) at a 90-m-resolution for 2015 (https://cgiarcsi.community/data/srtm-90m-digital-elevation-database-v4-1/). Monthly anthropogenic emissions of three atmospheric pollutants (e.g., sulfate dioxide (SO_2), black carbon (BC) and organic carbon (OC)) were from the Community Emissions Data System (CEDS, 1980–1999, http://www.globalchange.umd.edu/ceds/) and multi-resolution emission inventory for China (MEIC, 2000–2017 with 2018/2019 repeating 2017, http://www.meicmodel.org/) at a 0.5° × 0.667° spatial resolution. The population density in 2010 was obtained from LandScan at a 1-km-resolution (https://landscan.ornl.gov/landscan-datasets), which was also considered when constructing the emission inventories. We also apply the location of surface monitoring stations (longitude and latitude) and day of the year (DOY) as spatiotemporal information, with regard to the different spatial and temporal characteristics of $PM_{2.5}$.

2.2. Methods

Taking into account of the heterogeneous spatial and temporal distribution of $PM_{2.5}$ measurements, the STRF model, an upgraded Random Forest (RF) model with consideration of spatiotemporal information (Wei et al., 2019), is used in this study to produce long-term $PM_{2.5}$ data. RF is an ensemble learning algorithm on the basis of decision trees (DT) for classification and regression (Breiman, 2001). DT is a tree-structured classifier, which is recursively constructed by training data sets through dynamic programming (Safavian and Landgrebe, 1991). The major steps of RF algorithm (Joharestani et al., 2019) are as follows:

(a) N samples are collected from the data for training through bootstrap sampling method for individual trees.
(b) The RF model is built by utilizing the N samples generated from step (a). The split point of each tree is determined by the best feature among the randomly selected properties, which is capable of avoiding over-fitting.
(c) Tuning hyperparameters to optimize the performance of the model with K-fold CV technique.
(d) The estimated value of each input sample is then computed as the mean regression targets of the trees in the forest.

The following sections describe our concrete procedures of modeling $PM_{2.5}$:

Stage1. The $PM_{2.5}$ observation stations are grouped into 367 cities and the quality-controlled daily $PM_{2.5}$ concentrations are averaged for each city. Considering the mismatch of spatial distribution between

Table 1
Details of datasets used in this research.

Dataset	Variable	Content	Spatial resolution	Temporal resolution	Time period	Data source
$PM_{2.5}$	$PM_{2.5}$	Particulate matter ≤ 2.5 μm	Site	Hourly	2014–2019	CNEMC
VIS	VIS	Visibility	Site	Daily	1980–2019	NCDC
Meteorology	TEMP	Surface air temperature	Site	6 h	1980–2019	NCDC
	RH	Relative humidity		6 h	1980–2019	
	BLH	Boundary layer height	0.25° × 0.25°	6 h	1980–2019	ERA5
	SP	Surface pressure		6 h	1980–2019	
	ET	Evaporation		6 h	1980–2019	
	WS	10-m wind speed		6 h	1980–2019	
	WD	10-m wind direction		6 h	1980–2019	
Land use	LC	Land cover	300 m × 300 m	–	2015	ESA CCI
	NDVI	Normalized Difference Vegetation Index	0.05° × 0.05°	Daily	2015	AVHRR
Topography	TOPO	Digital elevation model	90 m × 90 m	–	2015	SRTM
Emission	SO_2	Sulfur dioxide	0.5° × 0.667°	Monthly	1980–2017	CEDS
	BC	Black carbon			1980–2017	MEIC
	OC	Organic carbon			1980–2017	
Population	POP	Population	1 km × 1 km	–	2010	LandScan

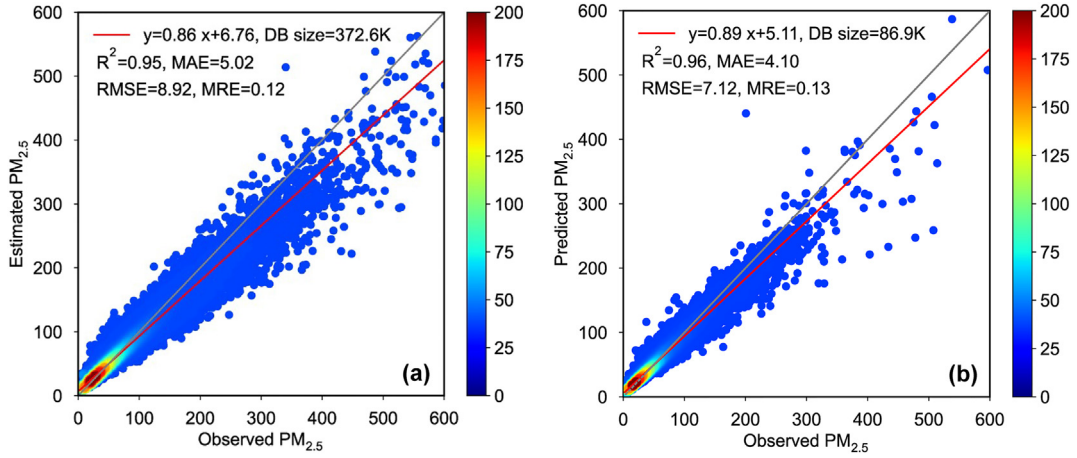

Fig. 2. Density scatterplot of (a) model fitting for the STRF model from 2014 to 2018 ($N = 372{,}596$) and (b) model prediction power in 2019 ($N = 86{,}871$) at the daily scale across China. The gray and red solid line is the 1:1 line and linear regression line, respectively. Statistical metrics including the correlation of determination (R^2), the root mean square error (RMSE), the mean absolute error (MAE) and the mean relative error (MRE) are noted at the top left of each panel. (For interpretation of the references to colour in this figure legend, the reader is referred to the web version of this article.)

visibility and $PM_{2.5}$ sites, we choose $\pm 1°$ around the geographic location of each city of $PM_{2.5}$ observation as a target area and average the corresponding visibility, in-situ TEMP and RH within the area. Totally 360 out of the 367 cities with $PM_{2.5}$ observations have visibility sites within their target areas. The other auxiliary data use values at the nearest grid to the city of $PM_{2.5}$ observation. We integrate all data but remove days with missing or invalid data for each geographic location.

Stage 2. The input datasets from 2014 to 2018 are used for model training. The hyperparameters applied in the machine learning model include n_estimators (the number of decision trees in the forest), min_samples_split (the minimum of samples required to split a node), max_features (the maximum number of features to consider when splitting a node), max_depth (the maximum depth of each decision tree) and bootstrap (an optional setting for sampling data with or without replacement). During the hyperparameter tuning to construct an optimized STRF model, the K-fold CV technique is applied to evaluate the skill of the STRF model. The K-fold CV splits the whole training data randomly into K subsets. In each round of CV among K rounds, K-1 subsets are used for fitting the model and the remaining subset is for validation, where K equals 10 in this study. The best hyperparameters of the model are 500, 4, "sqrt" (i.e., the maximum of features considered equals square root of all the features), "None" (i.e., the tree expands until the samples of each node are less than min_samples_split) and "Ture" (i.e., to turn on the boostrap option), respectively, for n_estimators, min_samples_split, max_features, max_depth and bootstrap. The average scores are used to identify best hyperparameters for the model. Several statistical metrics, including R^2, mean absolute error (MAE), root mean square error (RMSE) and mean relative error (MRE), are computed to measure the performance of the STRF model. Subsequently, the relationships between $PM_{2.5}$ concentrations and each independent parameter are investigated.

Stage 3. Using the regularly spaced visibility ground observation stations, we then process the daily visibility, meteorological data, land use, topography, anthropological emissions and population data from 1980 to 2019 according to the locations of valid visibility monitoring sites. The specifics of this procedure are the same as in stage 1. The long-term daily surface $PM_{2.5}$ concentrations over visibility sites during 1980–2019 are generated by the trained STRF model with input data of daily visibility, meteorological data, land use, topography, anthropological emissions, population, DOY and geographic location of visibility sites. Finally, the modeled data are interpolated into 1-degree grids over 1980–2019 in China using the bilinear interpolation method.

3. Results

3.1. Model performance and importance of input variables

Fig. 2a presents the density scatterplot of fitting performance of the STRF model. The validation data of daily surface $PM_{2.5}$ observations for model evaluation are 372,596 in total across China during 2014–2018. The STRF model slightly underestimates the $PM_{2.5}$ concentrations, with a slope of 0.86 in the regression model. The values of R^2, MAE, RMSE and MRE are 0.95, 5.02 μg/m^3, 8.92 μg/m^3 and 12%, respectively, indicating a good agreement between the estimated $PM_{2.5}$ and surface observations.

The prediction power of the STRF model is shown in Fig. 2b. The predicted daily $PM_{2.5}$ concentrations in 2019 are evaluated against 86,871 daily surface $PM_{2.5}$ measurements over China. The STRF model well reproduces the observational data with R^2, MAE, RMSE, and MRE of 0.96, 4.10 μg/m^3, 7.12 μg/m^3, and 13%, respectively. These statistical metrics demonstrate that the STRF model is a promising tool to estimate spatially coherent $PM_{2.5}$ concentrations that are crucial to study the long-term variability of $PM_{2.5}$ over China.

Fig. 3 shows the importance scores of 15 independent parameters used in the STRF model, which are calculated with all the input data

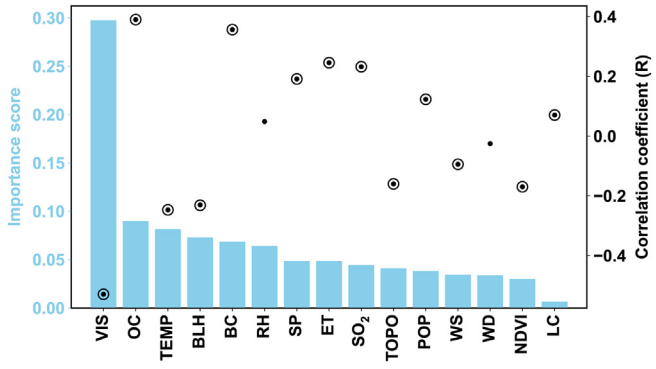

Fig. 3. Importance scores (y-axis on the left) of independent $PM_{2.5}$-related variables (OC, BC and SO_2 are for anthropogenic emissions) for the STRF model (blue bars) and correlation coefficients (y-axis on the right) between observed $PM_{2.5}$ concentrations and individual variables (black dots). Note that the concentric circles represent that correlation coefficients are statistically significant at the 95% confidence level. (For interpretation of the references to colour in this figure legend, the reader is referred to the web version of this article.)

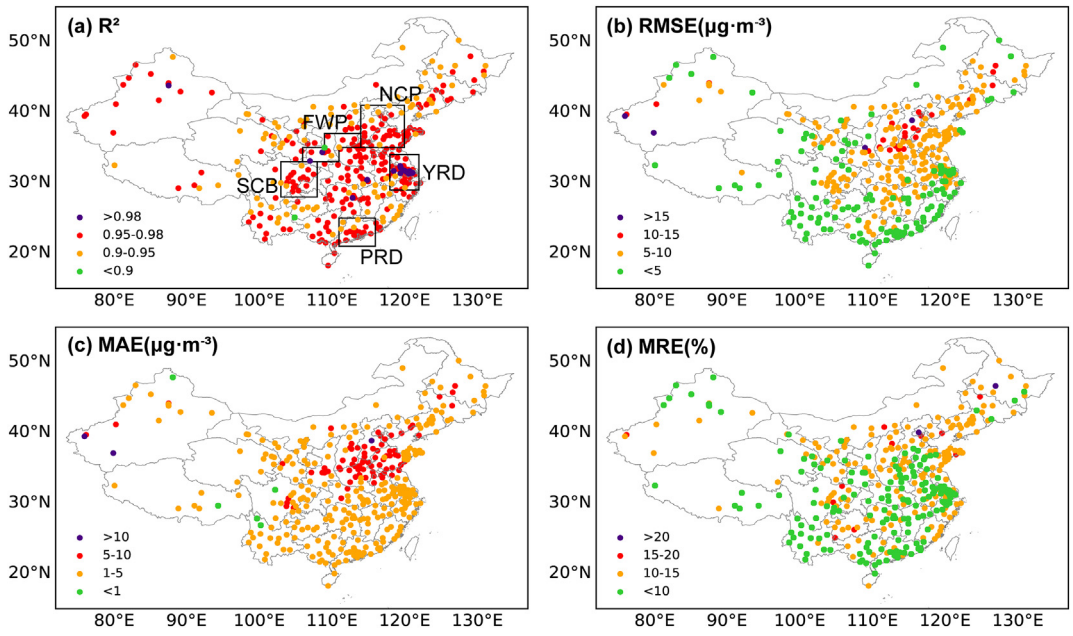

Fig. 4. Spatial distribution of the performance statistics of the STRF model according to (a) R^2 (unitless), (b) RMSE (μg m^{-3}), (c) MAE (μg m^{-3}) and (d) MRE (%) in 2014–2019 across China. The box-outlined areas in (a) are the North China Plain (NCP; 114–120°E, 35–41°N), the Fenwei Plain (FWP; 106–111°E, 33–35°N, and 109–114°E, 35–37°N), the Yangtze River Delta (YRD; 118–122°E, 29–34°N), the Pearl River Delta (PRD; 112–115°E, 21–25°N) and the Sichuan Basin (SCB; 103–108°E, 28–33°N).

considering both spatial and temporal variations, and the correlation coefficients (R) between these parameters and observed $PM_{2.5}$ concentrations are also provided. It is apparent that atmospheric visibility is the dominant parameter among all input variables, with an individual importance of 30% to the model, and it has a strong negative correlation with $PM_{2.5}$ observations ($R = -0.53$). TEMP and BLH are negatively correlated with $PM_{2.5}$, with the magnitude of R larger than 0.2. In contrast, all anthropogenic emissions and ET are positively correlated with $PM_{2.5}$, with R in the range of 0.2–0.4. Except for WD and RH, R between the selected variables and $PM_{2.5}$ concentrations is statistically significant at the 95% confidence level. In addition, emissions of OC and BC, TEMP, BLH and RH also significantly affect the $PM_{2.5}$ estimates, with individual contributions of 5–10% to the STRF model importance score.

3.2. Spatial and temporal validation

Fig. 4 shows the spatial validation of estimated $PM_{2.5}$ concentrations at city level across China during 2014–2019. In general, the daily $PM_{2.5}$ concentrations are well reproduced in most cities of China. Almost all cities have R^2 higher than 0.9. The average values of RMSE and MAE are 6.24 and 4.04 μg/m^3, respectively, with high values over North China Plain (NCP), Fenwei Plain (FWP) and northwestern China. About 87% (75%) of the cities have RMSE (MAE) less than 10 μg/m^3 (5 μg/m^3). The average of MRE is about 10% and more than 90% of the cities have MRE lower than 15%, particularly in east and south of China.

Fig. 5 shows the temporal model validation based on daily $PM_{2.5}$ concentrations averaged over China in 2014–2019. The spatial

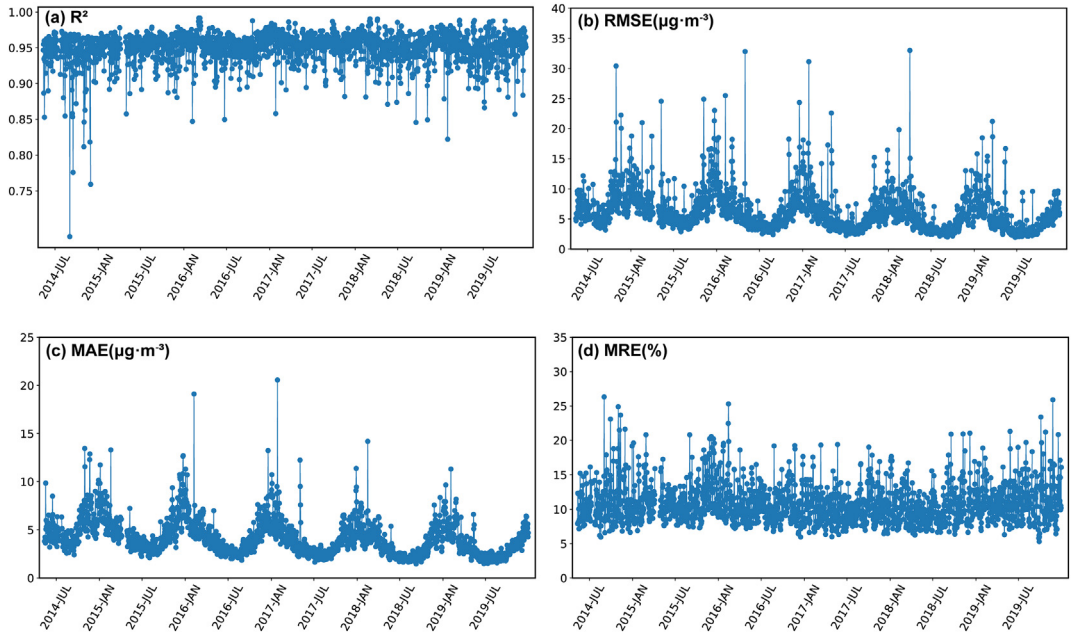

Fig. 5. The daily performance statistics of the STRF model averaged over China regarding to (a) R^2 (unitless), (b) RMSE (μg m^{-3}), (c) MAE (μg m^{-3}) and (d) MRE (%) in 2014–2019.

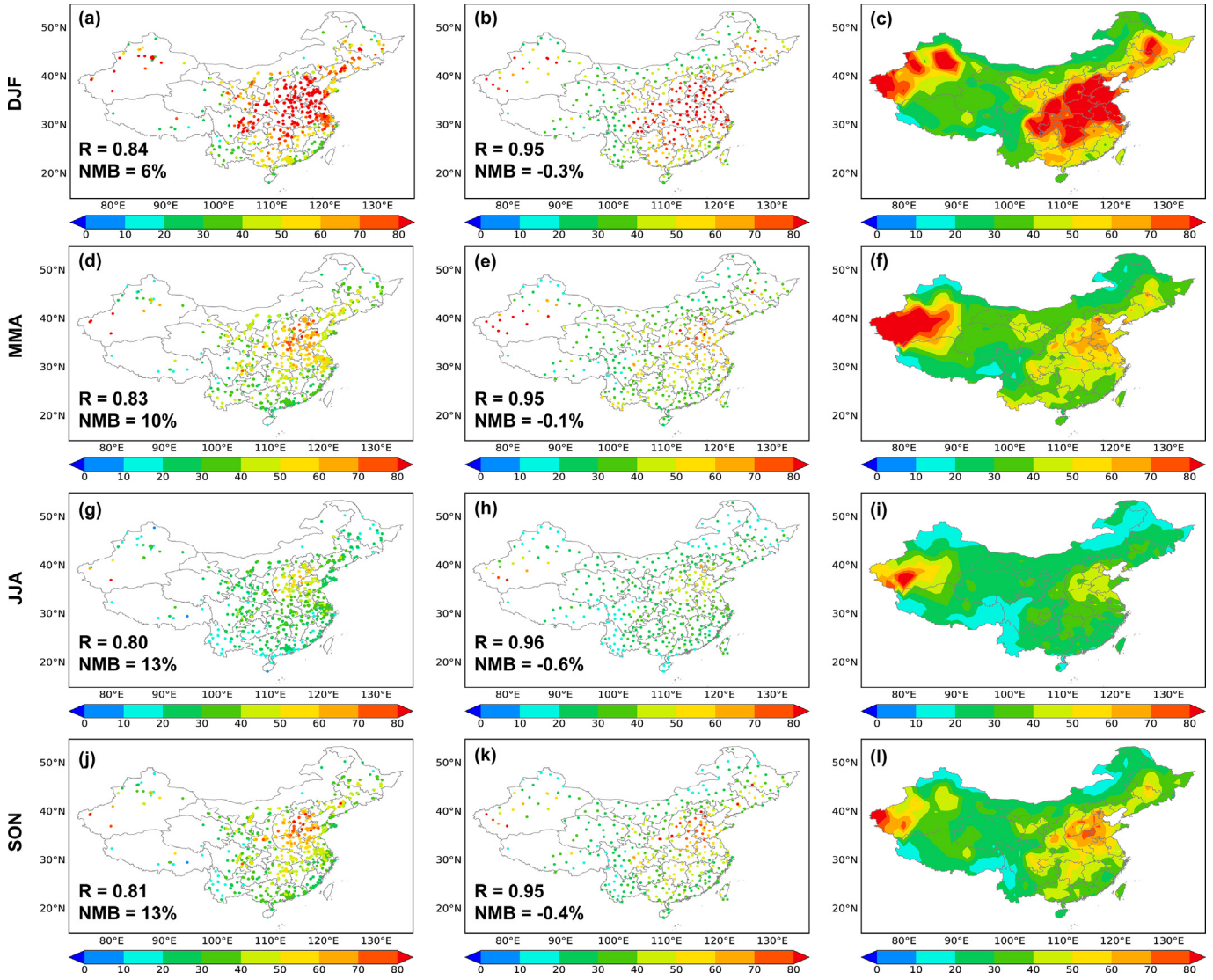

Fig. 6. Spatial distributions of observed surface $PM_{2.5}$ concentrations at 367 sites (a, d, g, j), $PM_{2.5}$ estimates from STRF model at 383 sites (b, e, h, k) and 1-degree gridded concentrations of $PM_{2.5}$ estimates (c, f, i, l) in 2015–2019 across China averaged over December–January–February (DJF), March–April–May (MAM), June–July–August (JJA) and September–October–November (SON). Correlation coefficient (R) and the normalized mean bias (NMB = $\sum$ ($Gridded_{site}$ − $Observation_{site}$) / $\sum Observation_{site}$ × 100% or NMB = $\sum$ ($Gridded_{site}$ − $Model_{site}$) / $Model_{site}$ × 100%) between gridded concentrations and $PM_{2.5}$ observations/model estimates are given at the bottom left of panels in left and middle columns.

distribution of modeled $PM_{2.5}$ is highly correlated with observed values with 88% of the days having R^2 higher than 0.9. More than 80% and 90% of the days have RMSE and MAE lower than 10 μg/m^3, with average values of 6.18 and 4.14 μg/m^3, respectively. The average of MRE is 11%, ranging from 5% to 26%, and 83% of the days have MRE lower than 15%. It is noteworthy that RMSE and MAE are higher in winter and lower in summer than other seasons. It is because the seasonal peak $PM_{2.5}$ concentrations usually occur in winter and trough occurs in summer over China, leading to larger absolute biases in cold season, which can be confirmed by the weaker seasonality of MRE.

3.3. Spatial distribution and seasonal variation of modeled $PM_{2.5}$

The observed $PM_{2.5}$ concentrations are typically higher in eastern China and lower in other less polluted regions. The modeled $PM_{2.5}$ concentrations at the 383 available visibility monitoring stations during 2015–2019 across China completely reproduce this spatial pattern (Fig. 6). Compared with the surface observations of $PM_{2.5}$, the modeled $PM_{2.5}$ based on visibility and other auxiliary data has a greater coverage over China, especially over the less polluted regions and areas of low popu lation density, which benefits the construction of gridded $PM_{2.5}$ data.

After being interpolated into the 1-degree gridded data using the bilinear interpolation method, the seasonal pattern of modeled $PM_{2.5}$ concentrations over 2015–2019 is also presented in Fig. 6. In eastern China, the $PM_{2.5}$ concentrations show peak in winter and trough in summer, with seasonal mean values above 80 μg/m^3 over most regions of eastern China in winter and around 40 μg/m^3 in summer, as a consequence of heating demands and unfavorable meteorological conditions in cold season and an efficient wet removal of aerosols in summer (Yang et al., 2017a, 2017b). In northwestern China, the severest particle pollution occurs in spring rather than winter since dust emissions increase dramatically and sandstorms occur frequently in these desert/arid areas in spring (Aili and Kim Oanh, 2015; Qiu et al., 2001). The dust variation is mainly driven by changes in wind speed and land cover (Yang et al., 2017c), which have been considered in the model. The overall R between the gridded $PM_{2.5}$ concentrations and observations are higher than 0.80, while the values of normalized mean bias (NMB) are less than 13%, suggesting that the constructed gridded $PM_{2.5}$ has an excellent representation of surface observations.

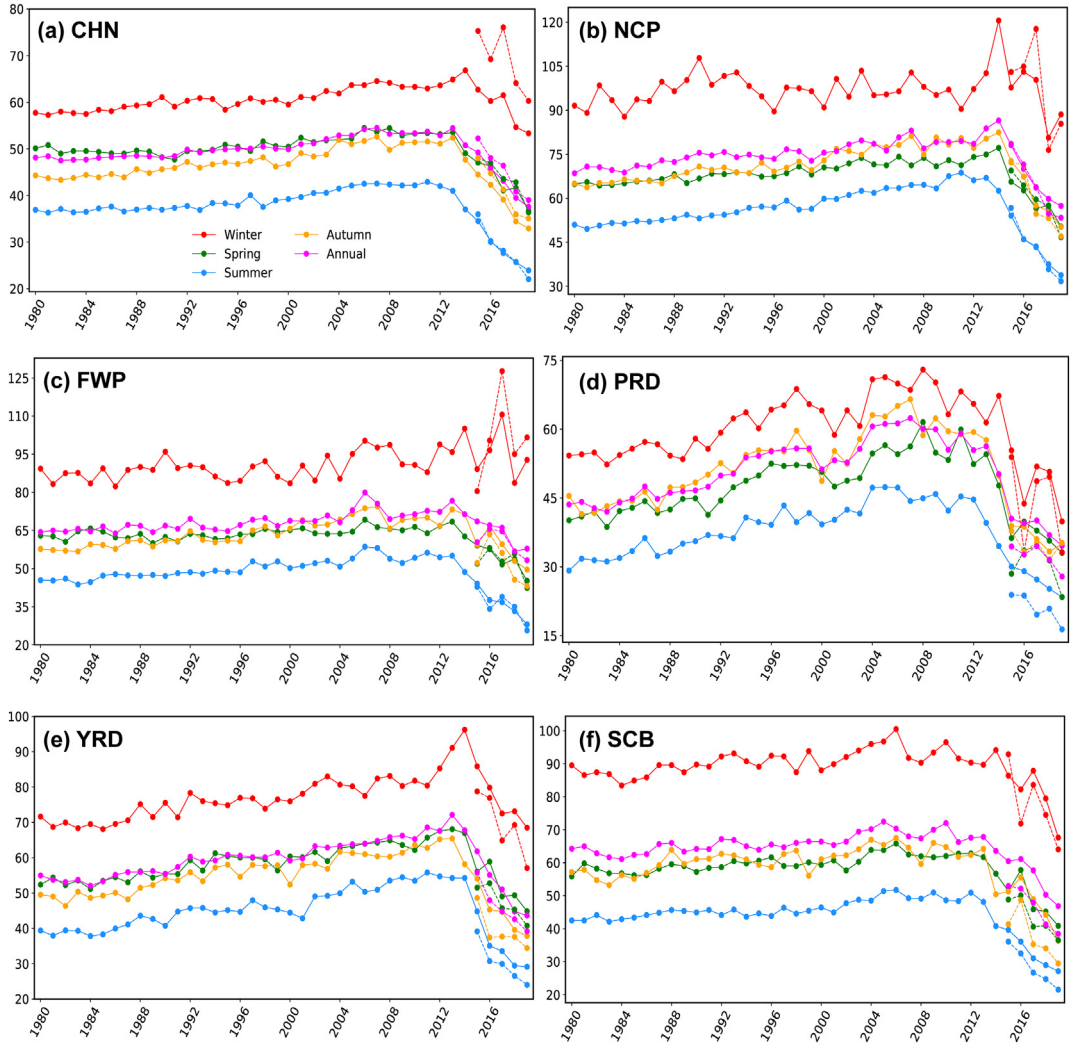

Fig. 7. Time series of annual mean (purple lines) and seasonal means of modeled $PM_{2.5}$ (colored solid lines) from 1980 to 2019 and corresponding observed $PM_{2.5}$ (colored dashed lines) from 2015 to 2019 averaged over China and five selected regions, including NCP, FWP, PRD, YRD and SCB. Note that the modeled mean is the average over all 1-degree grids while observed mean is only over stations. (For interpretation of the references to colour in this figure legend, the reader is referred to the web version of this article.)

3.4. Long-term variation of modeled $PM_{2.5}$

Using the trained STRF model along with long-term visibility and other auxiliary data, surface $PM_{2.5}$ concentrations during 1980–2019 over China can be reproduced, as shown in Fig. 7. As in Fig. 6, $PM_{2.5}$ concentrations are highest in winter and lowest in summer for the average over the whole China and five polluted areas of China, including NCP, FWP, the Yangtze River Delta (YRD), the Pearl River Delta (PRD) and the Sichuan Basin (SCB). NCP has the highest average $PM_{2.5}$ concentrations among the five sub-regions, with an annual mean concentration of 75.11 μg/m^3, followed by FWP (68.30 μg/m^3), SCB (66.07 μg/m^3), YRD (59.80 μg/m^3) and PRD (52.09 μg/m^3) from 1980 to 2013. Comparing to the surface observations (2015–2019), the model matches well the annual and spatial mean $PM_{2.5}$ concentrations.

Overall, the mean $PM_{2.5}$ shows a continuous increase during 1980–2013, mainly due to increases in anthropogenic emissions (Yang et al., 2016), and a rapid decrease during 2013–2019 resulting from the clean air actions in China (Zheng et al., 2018). Although $PM_{2.5}$ concentrations in all seasons and sub-regions show increasing trends in the first three decades after 1980 and decreasing trends from the 2010s, the peaks arrive at different years for different seasons and regions. For example, the wintertime maximum of national averaged $PM_{2.5}$ concentrations appears in 2014 (contributed by January and February of 2014 and December of 2013), while the summertime maximum occurs in 2011. In NCP, FWP and YRD, the annual $PM_{2.5}$ concentrations reach their maximum in 2013–2014, while the peak values show up in 2007 and 2010 over PRD and SCB, respectively. Note that the $PM_{2.5}$ concentrations over FWP have a high value in 2006, which is more likely a result of interannual variation and does not affect the increasing trend between 1980 and 2013.

3.5. Effect of clean air actions in China

From 1980–1984 to 2010–2014, the modeled 1-degree $PM_{2.5}$ concentrations increased in eastern China, with a maximum increase of more than 30 μg/m^3 occurred in Shanxi province, while $PM_{2.5}$ decreased in western China (Fig. 8). Since 2014, due to the clean air actions, $PM_{2.5}$ concentrations have decreased significantly throughout China. The decreases in $PM_{2.5}$ concentrations from 2010–2014 to 2015–2019 are in a similar magnitude to the increases during the past 30 years, with the maximum decrease of about 30 μg/m^3 over NCP.

Fig. 8e and f show the spatial distributions of linear trends of gridded $PM_{2.5}$ concentrations for 1980–2014 and 2014–2019, respectively. From 1980 to 2014, the $PM_{2.5}$ concentrations had increased at a maximum rate of 5–10 μg/m^3/decade in eastern China. As a result of the clean air actions, the $PM_{2.5}$ concentrations have decreased substantially in recent

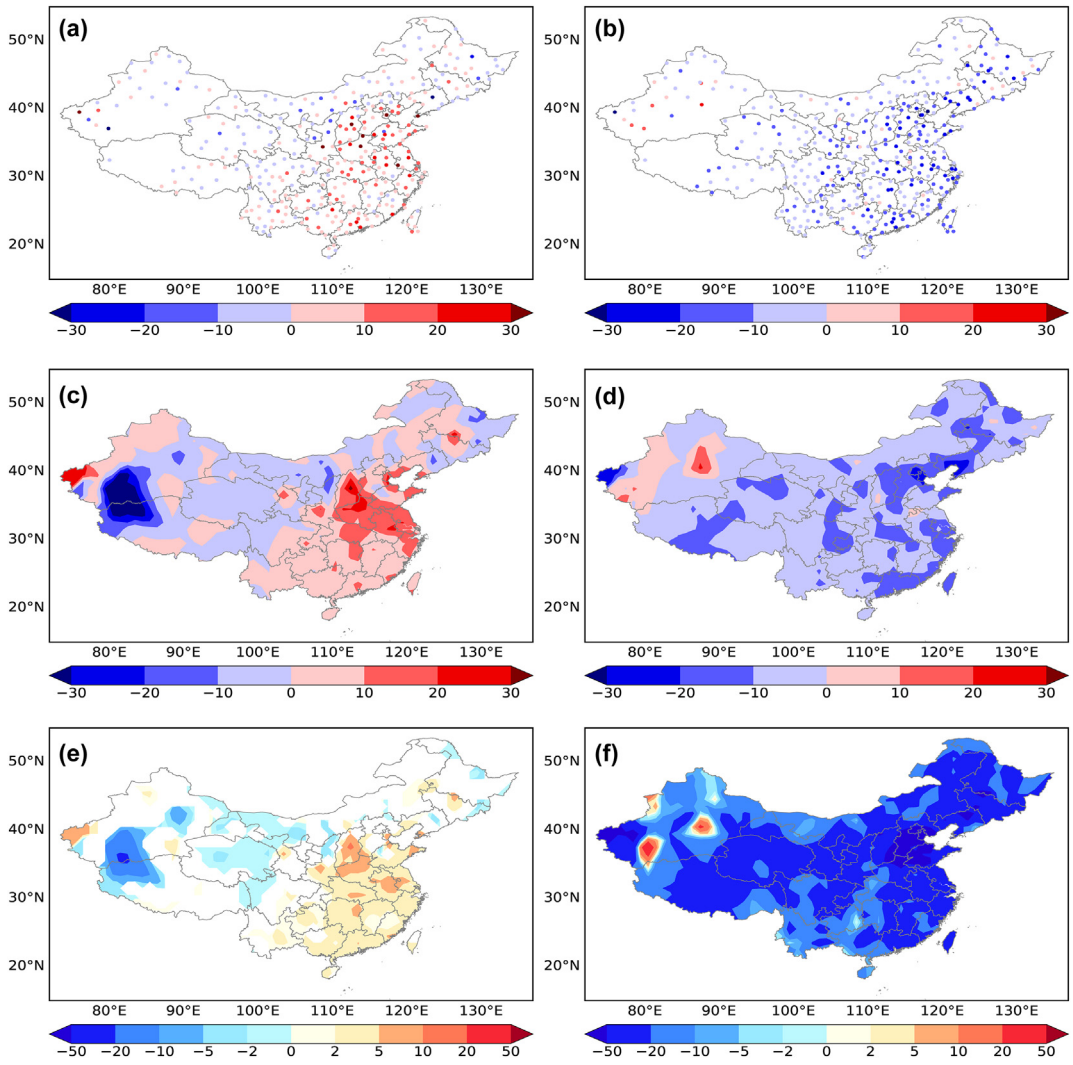

Fig. 8. Spatial distributions of differences in modeled 5-year mean station $PM_{2.5}$ concentrations and 1-degree gridded $PM_{2.5}$ concentrations between 1980–1984 and 2010–2014 (a, c) and between 2010–2014 and 2015–2019 (b, d), respectively. Linear trends of gridded $PM_{2.5}$ concentrations (μg/m^3/decade) for 1980–2014 (e) and 2014–2019 (f). Only areas with trends passing significant test at the 99% confidence level are drawn in e and f.

years, with a reduction rate of over 50 μg/m^3/decade in the North China Plain and 20–50 μg/m^3/decade in many regions of China, which is approximately one order of magnitude faster than the increasing rate over 1980–2014 in eastern China. It is also noted that an increasing trend of $PM_{2.5}$ occurred over northwestern China in 2014–2019, which is likely caused by interannual variations in dust emissions.

4. Conclusion and discussions

In this study, the STRF machine learning model is trained with the input of atmospheric visibility observations, meteorology, land use, topography, anthropogenic emissions, population, and relevant spatiotemporal information to construct a 1-degree gridded near-surface daily $PM_{2.5}$ concentration dataset from 1980 to 2019. This spatiotemporally coherent historical $PM_{2.5}$ dataset is useful to study the long-term aerosol variations over China.

The $PM_{2.5}$ estimates are well correlated with near-surface observations over China for 2014–2018, with a relatively high R^2 of 0.95 and low values of MAE of 4.84 μg/m^3, RMSE of 8.61 μg/m^3 and MRE of 12%. Among the 15 selected individual variables, atmospheric visibility is the dominant factor, which accounts for 30% of the total importance score in estimating $PM_{2.5}$ by the model. Besides, emissions (e.g., OC and BC) and meteorological conditions (e.g., TEMP, BLH and RH) are also essential factors, each explaining 5–10% of the total importance. The constructed $PM_{2.5}$ concentrations show high values in eastern China and low values in the less polluted regions, such as western China, and seasonal peak in winter and trough in summer, which have very similar spatiotemporal patterns to observations.

From 1980 to 2014, the model-predicted $PM_{2.5}$ concentrations increased constantly over eastern China, where anthropogenic emissions were increasing during this time period, with the maximum growth rate of 5–10 μg/m^3/decade. After the implementation of the clean air actions, the air quality across China has improved enormously during 2014–2019, with a decreasing rate over 50 μg/m^3/decade for $PM_{2.5}$ concentrations in the NCP and 20–50 μg/m^3/decade over many regions of China, which is approximately one order of magnitude faster than the increasing rate during 1980–2014.

Numerous previous studies have estimated $PM_{2.5}$ concentrations in China based on satellite-retrieved column AOD. However, due to the limitations in time coverage and satellite retrieval algorithms, the estimated $PM_{2.5}$ concentrations are only available after 2000 and not representative for the surface. With the long-term visibility and auxiliary data, the machine learning estimated $PM_{2.5}$ data is constructed for the recent four decades (1980–2019). The newly produced 1-degree gridded daily $PM_{2.5}$ dataset in China is useful to complement satellite-based $PM_{2.5}$ products and provide information over remote areas

where $PM_{2.5}$ monitoring stations are scarce. As a consequence, our long-term 1-degree gridded $PM_{2.5}$ dataset can be a practical tool for analyzing the long-term variation of aerosols in China and assisting air quality and climate models to assess related impacts on environment and climate.

There are complex correlations between the input variables, but the covariations of these variables are hard to be considered in the traditional statistical methods. For example, the R is 0.45 between boundary layer height and wind speed, 0.48 between population and SO_2 emission, and 0.30 between surface air temperature and relative humidity. Due to the better abilities in dealing with non-linear and complex relationships between variables, machine learning method is used in this study. However, there are a few uncertainties associated with the results in this study. For example, uncertainties exist in the $PM_{2.5}$ and visibility observations, meteorological reanalysis data, and the prescribed anthropogenic aerosol emissions. Additionally, some auxiliary data have spatial variation but are lack of temporal variation. For example, land use, topography and population density are only for one specific year and the aerosol and precursor emissions are monthly mean values. The constructed daily $PM_{2.5}$ concentrations could be biased without considering daily variation of these variables. Due to the fact that Tibetan Plateau and parts of western China have less dense observation stations compared to eastern China, uncertainties can be induced in the model training and data interpolation. Therefore, the constructed dataset of gridded $PM_{2.5}$ concentrations is likely to be less reliable in western China than in eastern China. Moreover, in processing the input data, days with precipitation and high RH were removed, which could cause a high bias in calculating the annual average of $PM_{2.5}$. The potential model dependence of $PM_{2.5}$ simulation warrants a further study with multiple machine learning models and more input data.

CRediT authorship contribution statement

Huimin Li: Conceptualization, Data curation, Formal analysis, Investigation, Methodology, Software, Visualization, Writing – original draft. **Yang Yang:** Conceptualization, Data curation, Formal analysis, Project administration, Supervision, Writing – review & editing. **Hailong Wang:** Formal analysis, Writing – review & editing. **Baojie Li:** Data curation. **Pinya Wang:** Data curation, Formal analysis. **Jiandong Li:** Data curation. **Hong Liao:** Writing – review & editing.

Declaration of competing interest

The authors declare that they have no known competing financial interests or personal relationships that could have appeared to influence the work reported in this paper.

Acknowledgments

This study was supported by the National Natural Science Foundation of China (grant 41975159) and the National Key Research and Development Program of China (grant 2020YFA0607803 and 2019YFA0606800). HW acknowledges the support by the U.S. Department of Energy (DOE), Office of Science, Office of Biological and Environmental Research (BER), as part of the Earth and Environmental System Modeling program. The Pacific Northwest National Laboratory (PNNL) is operated for DOE by the Battelle Memorial Institute under contract DE-AC05-76RLO1830. The constructed 1-degree gridded $PM_{2.5}$ data are available at https://zenodo.org/record/4293239.

References

Aili, A., Kim Oanh, N.T., 2015. Effects of dust storm on public health in desert fringe area: case study of northeast edge of Taklimakan Desert, China. Atmos. Pollut. Res. 6, 805–814. https://doi.org/10.5094/APR.2015.089.

Barrero, M.A., Orza, J.A.G., Cabello, M., Cantón, L., 2015. Categorisation of air quality monitoring stations by evaluation of PM_{10} variability. Sci. Total Environ. 524–525, 225–236. https://doi.org/10.1016/j.scitotenv.2015.03.138.

Boucher, O., Randall, D., Artaxo, P., Bretherton, C., Feingold, G., Forster, P., Kerminen, V.M., Kondo, Y., Liao, H., Lohmann, U., Rasch, P., Satheesh, S.K., Sherwood, S., Stevens, B., Zhang, X., 2013. Clouds and aerosols. In Climate change 2013: The physical science basis. Contribution of working group I to the fifth assessment report of the intergovernmental panel on climate change. Stocker, T.F., Qin, D., Plattner, G.K., Tignor, M., Allen, S.K., Boschung, J., Nauels, A., Xia, Y., Bex, V., Midgley, P.M. (Eds.), Cambridge University Press., Cambridge, U.K. and New York, USA, pp. 571–657.

Breiman, L., 2001. Random forests. Mach. Learn. 45, 5–32. doi:10.1023/A:1010933404324.

Chelani, A.B., 2019. Estimating $PM_{2.5}$ concentration from satellite derived aerosol optical depth and meteorological variables using a combination model. Atmos. Pollut. Res. 10, 847–857. https://doi.org/10.1016/j.apr.2018.12.013.

CMA, 2014. Forecasting and Networking Department of China Meteorological Administration released letter No.4: Notice on the adjustments of the haze weather phenomenon observation and on the revision of the fog and haze observation data.

Cohen, A.J., Brauer, M., Burnett, R., Anderson, H.R., Frostad, J., Estep, K., Balakrishnan, K., Brunekreef, B., Dandona, L., Dandona, R., Feigin, V., Freedman, G., Hubbell, B., Jobling, A., Kan, H., Knibbs, L., Liu, Y., Martin, R., Morawska, L., Pope, C.A., Shin, H., Straif, K., Shaddick, G., Thomas, M., van Dingenen, R., van Donkelaar, A., Vos, T., Murray, C.J.L., Forouzanfar, M.H., 2017. Estimates and 25-year trends of the global burden of disease attributable to ambient air pollution: an analysis of data from the global burden of diseases study 2015. Lancet 389, 1907–1918. https://doi.org/10.1016/S0140-6736(17)30505-6.

Crouse, D.L., Peters, P.A., van Donkelaar, A., Goldberg, M.S., Villeneuve, P.J., Brion, O., Khan, S., Atari, D.O., Jerrett, M., Pope, C.A., Brauer, M., Brook, J.R., Martin, R.V., Stieb, D., Burnett, R.T., 2012. Risk of nonaccidental and cardiovascular mortality in relation to long-term exposure to low concentrations of fine particulate matter: a Canadian national-level cohort study. Environ. Health Perspect. 120, 708–714. https://doi.org/10.1289/ehp.1104049.

van Donkelaar, A., Martin, R.V., Brauer, M., Boys, B.L., 2015. Use of satellite observations for long-term exposure assessment of global concentrations of fine particulate matter. Environ. Health Perspect. 123, 135–143. https://doi.org/10.1289/ehp.1408646.

Fang, X., Zou, B., Liu, X., Sternberg, T., Zhai, L., 2016. Satellite-based ground $PM_{2.5}$ estimation using timely structure adaptive modeling. Remote Sens. Environ. 186, 152–163. https://doi.org/10.1016/j.rse.2016.08.027.

Gui, K., Che, H., Zeng, Z., Wang, Y., Zhai, S., Wang, Z., Luo, M., Zhang, L., Liao, T., Zhao, H., Li, L., Zheng, Y., Zhang, X., 2020. Construction of a virtual PM2.5 observation network in China based on high-density surface meteorological observations using the Extreme Gradient Boosting model. Environ. Int. 141, 105801. https://doi.org/10.1016/j.envint.2020.105801.

Guo, Y., Tang, Q., Gong, D., Zhang, Z., 2017. Estimating ground-level $PM_{2.5}$ concentrations in Beijing using a satellite-based geographically and temporally weighted regression model. Remote Sens. Environ. 198, 140–149. https://doi.org/10.1016/j.rse.2017.06.001.

Huang, J., Pan, X., Guo, X., Li, G., 2018. Health impact of China's Air Pollution Prevention and Control Action Plan: an analysis of national air quality monitoring and mortality data. Lancet Planet. Health 2, 313–323. https://doi.org/10.1016/S2542-5196(18)30141-4.

Joharestani, M.Z., Cao, C., Ni, X., Bashir, B., Talebiesfandarani, S., 2019. $PM_{2.5}$ prediction based on random forest, XGBoost, and deep learning using multisource remote sensing data. Atmosphere 10, 373. https://doi.org/10.3390/atmos10070373.

Li, T., Shen, H., Yuan, Q., Zhang, X., Zhang, L., 2017. Estimating ground-level $PM_{2.5}$ by fusing satellite and station observations: a geo-intelligent deep learning approach. Geophys. Res. Lett. 44, 11985–11993. https://doi.org/10.1002/2017gl075710.

Li, S., Chen, L., Huang, G., Lin, J., Yan, Y., Ni, R., Huo, Y., Wang, J., Liu, M., Weng, H., Wang, Y., Wang, Z., 2020. Retrieval of surface $PM_{2.5}$ mass concentrations over North China using visibility measurements and GEOS-Chem simulations. Atmos. Environ. 222, 117121. https://doi.org/10.1016/j.atmosenv.2019.117121.

Liu, Y., Paciorek, C.J., Koutrakis, P., 2009. Estimating regional spatial and temporal variability of $PM_{2.5}$ concentrations using satellite data, meteorology, and land use information. Environ. Health Perspect. 117, 886–892. https://doi.org/10.1289/ehp.0800123.

Liu, M., Bi, J., Ma, Z., 2017. Visibility-based $PM_{2.5}$ concentrations in China: 1957–1964 and 1973–2014. Environ. Sci. Technol. 51, 13161–13169. https://doi.org/10.1021/acs.est.7b03468.

Ma, Z., Hu, X., Huang, L., Bi, J., Liu, Y., 2014. Estimating ground-level $PM_{2.5}$ in China using satellite remote sensing. Environ. Sci. Technol. 48, 7436–7444. https://doi.org/10.1021/es5009399.

Ma, Z., Hu, X., Sayer, A.M., Levy, R., Zhang, Q., Xue, Y., Tong, S., Bi, J., Huang, L., Liu, Y., 2016. Satellite-based spatiotemporal trends in $PM_{2.5}$ concentrations: China, 2004–2013. Environ. Health Perspect. 124, 184–192. https://doi.org/10.1289/ehp.1409481.

Pant, P., Guttikunda, S.K., Peltier, R.E., 2016. Exposure to particulate matter in India: a synthesis of findings and future directions. Environ. Res. 147, 480–496. https://doi.org/10.1016/j.envres.2016.03.011.

Pope, C.A., Burnett, R.T., Thun, M.J., Calle, E.E., Krewski, D., Ito, K., Thurston, G.D., 2002. Lung cancer, cardiopulmonary mortality, and long-term exposure to fine particulate air pollution. Jama J. Am. Med. Assoc. 287, 1132–1141. https://doi.org/10.1001/jama.287.9.1132.

Qiu, X., Zeng, Y., Miao, Q., 2001. Sand-dust storms in China: temporal-spatial distribution and tracks of source lands. J. Geogr. Sci. 11, 253–260. https://doi.org/10.1007/BF02892308.

Ren, L., Yang, Y., Wang, H., Zhang, R., Wang, P., Liao, H., 2020. Source attribution of Arctic black carbon and sulfate aerosols and associated Arctic surface warming during 1980–2018. Atmos. Chem. Phys. 20, 9067–9085. https://doi.org/10.5194/acp-20-9067-2020.

Safavian, S.R., Landgrebe, D., 1991. A survey of decision tree classifier methodology. IEEE Trans. Syst. Man Cybern. 21, 660–674.

Shen, Z., Cao, J., Zhang, L., Zhang, Q., Huang, R.J., Liu, S., Zhao, Z., Zhu, C., Lei, Y., Xu, H., Zheng, C., 2016. Retrieving historical ambient $PM_{2.5}$ concentrations using existing visibility measurements in Xi'an, Northwest China. Atmos. Environ. 126, 15–20. https://doi.org/10.1016/j.atmosenv.2015.11.040.

Stafoggia, M., Bellander, T., Bucci, S., Davoli, M., de' Hoogh, K., de Donato, F., Gariazzo, C., Lyapustin, A., Michelozzi, P., Renzi, M., Scortichini, M., Shtein, A., Viegi, G., Kloog, I., Schwartz, J., 2019. Estimation of daily PM_{10} and $PM_{2.5}$ concentrations in Italy, 2013–2015, using a spatiotemporal land-use random-forest model. Environ. Int. 124, 170–179. https://doi.org/10.1016/j.envint.2019.01.016.

Wang, Y., Zhang, R., Saravanan, R., 2014. Asian pollution climatically modulates mid-latitude cyclones following hierarchical modeling and observational analysis. Nat. Commun. 5, 3098. https://doi.org/10.1038/ncomms4098.

Wang, W., Zhao, S., Jiao, L., Taylor, M., Zhang, B., Xu, G., Hou, H., 2019. Estimation of $PM_{2.5}$ concentrations in China using a spatial back propagation neural network. Sci. Rep. 9, 1–10. https://doi.org/10.1038/s41598-019-50177-1.

Wei, J., Huang, W., Li, Z., Xue, W., Peng, Y., Sun, L., Cribb, M., 2019. Estimating 1-km-resolution $PM_{2.5}$ concentrations across China using the space-time random forest approach. Remote Sens. Environ. 231, 111221. https://doi.org/10.1016/j.rse.2019.111221.

Wei, J., Li, Z., Cribb, M., Huang, W., Xue, W., Sun, L., Guo, J., Peng, Y., Li, J., Lyapustin, A., Liu, L., Wu, H., Song, Y., 2020. Improved 1 km resolution $PM_{2.5}$ estimates across China using enhanced space-time extremely randomized trees. Atmos. Chem. Phys. 20, 3273–3289. https://doi.org/10.5194/acp-20-3273-2020.

Xiao, Q., Wang, Y., Chang, H.H., Meng, X., Geng, G., Lyapustin, A., Liu, Y., 2017. Full-coverage high-resolution daily $PM_{2.5}$ estimation using MAIAC AOD in the Yangtze River Delta of China. Remote Sens. Environ. 199, 437–446. https://doi.org/10.1016/j.rse.2017.07.023.

Xing, Y., Xu, Y., Shi, M., Lian, Y., 2016. The impact of $PM_{2.5}$ on the human respiratory system. J. Thorac. Dis. 8, 69–74. https://doi.org/10.3978/j.issn.2072-1439.2016.01.19.

Xue, T., Zheng, Y., Tong, D., Zheng, B., Li, X., Zhu, T., Zhang, Q., 2019. Spatiotemporal continuous estimates of $PM_{2.5}$ concentrations in China, 2000–2016: a machine learning method with inputs from satellites, chemical transport model, and ground observations. Environ. Int. 123, 345–357. https://doi.org/10.1016/j.envint.2018.11. 075.

Yang, Y., Liao, H., Lou, S., 2016. Increase in winter haze over eastern China in recent decades: roles of variations in meteorological parameters and anthropogenic emissions. J. Geophys. Res. Atmos. 121, 13050–13065. https://doi.org/10.1002/2016JD025136.

Yang, Y., Wang, H., Smith, S.J., Zhang, R., Lou, S., Qian, Y., Ma, P.-L., Rasch, P.J., 2017a. Recent intensification of winter haze in China linked to foreign emissions and meteorology. Sci. Rep. 8, 2107. https://doi.org/10.1038/s41598-018-20437-7.

Yang, Y., Wang, H., Smith, S.J., Ma, P.-L., Rasch, P.J., 2017b. Source attribution of black carbon and its direct radiative forcing in China. Atmos. Chem. Phys. 17, 4319–4336. https://doi.org/10.5194/acp-17-4319-2017.

Yang, Y., Russell, L.M., Lou, S., Liao, H., Guo, J., Liu, Y., Singh, B., Ghan, S.J., 2017c. Dust-wind interactions can intensify aerosol pollution over eastern China. Nat. Commun. 8, 15333. https://doi.org/10.1038/ncomms15333.

Yang, Y., Ren, L., Li, H., Wang, H., Wang, P., Chen, L., Yue, X., Liao, H., 2020. Fast climate responses to aerosol emission reductions during the COVID-19 pandemic. Geophys. Res. Lett. 47, e2020GL089788. https://doi.org/10.1029/2020GL089788.

Yao, F., Wu, J., Li, W., Peng, J., 2019. A spatially structured adaptive two-stage model for retrieving ground-level $PM_{2.5}$ concentrations from VIIRS AOD in China. ISPRS J. Photogramm. Remote Sens. 151, 263–276. https://doi.org/10.1016/j.isprsjprs.2019.03.011.

Zhai, S., Jacob, D.J., Wang, X., Shen, L., Li, K., Zhang, Y., Gui, K., Zhao, T., Liao, H., 2019. Fine particulate matter ($PM_{2.5}$) trends in China, 2013–2018: separating contributions from anthropogenic emissions and meteorology. Atmos. Chem. Phys. 19, 11031–11041. https://doi.org/10.5194/acp-19-11031-2019.

Zhang, R., Li, Q., Zhang, R., 2014. Meteorological conditions for the persistent severe fog and haze event over eastern China in January 2013. Sci. China Earth Sci. 57, 26–35. https://doi.org/10.1007/s11430-013-4774-3.

Zhang, Q., Jiang, X., Tong, D., Davis, S.J., Zhao, H., Geng, G., Feng, T., Zheng, B., Lu, Z., Streets, D.G., Ni, R., Brauer, M., van Donkelaar, A., Martin, R.V., Huo, H., Liu, Z., Pan, D., Kan, H., Yan, Y., Lin, J., He, K., Guan, D., 2017. Transboundary health impacts of transported global air pollution and international trade. Nature 543, 705–709. https://doi.org/10.1038/nature21712.

Zhao, C., Wang, Q., Ban, J., Liu, Z., Zhang, Y., Ma, R., Li, S., Li, T., 2020. Estimating the daily $PM_{2.5}$ concentration in the Beijing-Tianjin-Hebei region using a random forest model with a $0.01^\circ \times 0.01^\circ$ spatial resolution. Environ. Int. 134, 105297. https://doi.org/10.1016/j.envint.2019.105297.

Zheng, Y., Zhang, Q., Liu, Y., Geng, G., He, K., 2016. Estimating ground-level $PM_{2.5}$ concentrations over three megalopolises in China using satellite-derived aerosol optical depth measurements. Atmos. Environ. 124, 232–242. https://doi.org/10.1016/j.atmosenv.2015.06.046.

Zheng, B., Tong, D., Li, M., Liu, F., Hong, C., Geng, G., Li, H., Li, X., Peng, L., Qi, J., Yan, L., Zhang, Y., Zhao, H., Zheng, Y., He, K., Zhang, Q., 2018. Trends in China's anthropogenic emissions since 2010 as the consequence of clean air actions. Atmos. Chem. Phys. 18, 14095–14111. https://doi.org/10.5194/acp-18-14095-2018.